DOES THE OOSTERHOFF DICHOTOMY EXIST IN THE ANDROMEDA GALAXY? I. THE CASE OF G11[*]

Rodrigo Contreras Ramos[1,2,3], Gisella Clementini[1], Luciana Federici[1], Giuliana Fiorentino[1],
Carla Cacciari[1], Márcio Catelan[3,4], Horace A. Smith[5], Flavio Fusi Pecci[1], Marcella Marconi[6],
Barton J. Pritzl[7], and Karen Kinemuchi[8]

[1] INAF, Osservatorio Astronomico di Bologna, Bologna, Italy; rodrigo.contreras@oabo.inaf.it, gisella.clementini@oabo.inaf.it, luciana.federici@oabo.inaf.it,
giuliana.fiorentino@oabo.inaf.it, carla.cacciari@oabo.inaf.it, flavio.fusipecci@oabo.inaf.it
[2] Dipartimento di Astronomia, Università di Bologna, Bologna, Italy
[3] Pontificia Universidad Católica de Chile, Departamento de Astronomía y Astrofísica, Santiago, Chile; mcatelan@astro.puc.cl
[4] The Milky Way Millennium Nucleus, Av. Vicuña Mackenna 4860, 782-0436 Macul, Santiago, Chile
[5] Department of Physics and Astronomy, Michigan State University, East Lansing, MI 48824, USA; smith@pa.msu.edu
[6] INAF, Osservatorio Astronomico di Capodimonte, Napoli, Italy; marcella@na.astro.it
[7] Department of Physics and Astronomy, University of Wisconsin Oshkosh, Oshkosh, WI 54901, USA; pritzlb@uwosh.edu
[8] Apache Point Observatory/New Mexico State University, Sunspot, NM 88349, USA; kinemuchi@apo.nmsu.edu

ABSTRACT

We present the first evidence that Oosterhoff type II globular clusters exist in the Andromeda galaxy (M31). On the basis of time-series photometry of the moderately metal-poor ([Fe/H] ~ -1.6 dex) M31 globular cluster G11, obtained with the Wide Field Planetary Camera 2 on board the *Hubble Space Telescope*, we detected and derived periods for 14 RR Lyrae stars, of which five are found to lie inside the cluster tidal radius. They include three fundamental-mode (RRab) and two first-overtone (RRc) pulsators, with average periods $\langle P_{ab} \rangle = 0.70$ days, and $\langle P_c \rangle = 0.40$ days, respectively. These mean periods and the position of the cluster variable stars in the period–amplitude and period–metallicity diagrams all suggest that G11 is likely to be an Oosterhoff type II globular cluster. This appears to be in agreement with the general behavior of Milky Way globular clusters with similar metallicity and horizontal branch morphology.

Key words: galaxies: individual (M31) – globular clusters: individual (G11) – stars: distances – stars: variables:
RR Lyrae – techniques: photometric

Online-only material: color figures, machine-readable table

1. INTRODUCTION

More than seventy years ago, Oosterhoff (1939) discovered that the Milky Way (MW) globular clusters (GCs) could be divided into two groups according to the mean period of their RR Lyrae (RRL) stars. The two groups were later christened according to his name, Oosterhoff type I (Oo I) and Oosterhoff type II (Oo II; see, e.g., Preston 1959). Oo I clusters contain fundamental-mode RRL stars (RRab) with a mean period, $\langle P_{ab} \rangle$, close to 0.55 days, while Oo II clusters contain RRab's with mean period close to 0.65 days. Differences in the mean period of the first-overtone RRL stars (RRc) in these clusters were also present. Oo I clusters had the RRc mean period, $\langle P_c \rangle$, near 0.32 days, while GCs classified as Oo II showed $\langle P_c \rangle \sim 0.37$ days. He also noted that the percentage of c-type variables differed between the two groups, with the RRL population of the Oo I clusters being largely dominated by ab-type pulsators ($f_c = N_c/N_{ab+c} \sim 0.17$, where N_c and N_{ab} are the numbers of first-overtone and fundamental-mode RRL stars, respectively), whereas Oo II clusters generally contained a more balanced proportion of c- to ab-type pulsators ($f_c \sim 0.44$). However, one should be aware that incompleteness and selection effects may alter this property (Smith 1995). Subsequent studies (Oosterhoff 1944; Sawyer 1944) including new RRL-rich GCs soon confirmed the dichotomy. When metal abundances began to be measured for GCs, it became clear that the two Oo

groups showed differences also in metallicity. Oo I clusters were moderately metal-poor ([Fe/H] ~ -1.3 dex), while Oo II clusters were very metal-poor ([Fe/H] ~ -2.0 dex). Recent studies (see, e.g., Catelan 2009, for a review) involving larger samples of GCs, more accurate metallicities, better periods for the RRL stars, and higher completeness, have fully confirmed the Oosterhoff dichotomy not only among the Galactic GCs (GGCs), but also for field variable stars in the MW halo (see, e.g., Miceli et al. 2008). On the other hand, extragalactic GCs and field RRL stars in the Local Group dwarf galaxies generally have $\langle P_{ab} \rangle$ ranging between 0.58 days and 0.62 days, thus they preferentially occupy the so-called Oosterhoff gap avoided by the MW GCs, and are classified as Oosterhoff-Intermediate (Oo-Int; Catelan 2009; Clementini 2010, and references therein).[9] This very straightforward observational evidence bears very significant implications on our understanding of the Galactic halo formation. Indeed, if the Galactic halo was assembled by capture of "building blocks" resembling the bright dwarf galaxies we see today around the MW, then the properties of their RRL stars should conform to the Oosterhoff dichotomy we observe for the MW field and cluster stars. The absence of an Oosterhoff dichotomy, along with differences in the chemical abundances (e.g., Shetrone et al. 2001, Helmi et al. 2006), thus seem to rule out the bright dwarf galaxies surrounding the MW as significant contributors to the assembling of the Galactic halo (e.g., Catelan 2004, 2009).

---

[9] Among the bright dwarf spheroidal (dSph) companions of the MW, only Ursa Minor with $\langle P_{ab} \rangle \sim 0.64$ days has Oo II properties, and Sagittarius with $\langle P_{ab} \rangle \sim 0.574$ days is on the long period tail of the Oo I group (see, e.g., Cseresnjes 2001).

Table 1
Basic Parameters of the Target M31 Clusters, Taken from RBC V4.0

Name	V (mag)	$(B-V)$ (mag)	[Fe/H][a]	[Fe/H]$_{C09}$[a]	X (arcmin)	Y (arcmin)	R (kpc)
B293-G011	16.30	0.33	−1.59	−1.60	−61.86	43.64	17.24
B311-G033	15.45	0.96	−1.71	−1.73	−57.57	0.99	13.11
B338-G076	14.25	0.81	−1.23	−1.20	−44.09	−9.05	10.25
B343-G105	16.31	0.77	−1.28	−1.25	−57.45	−30.05	14.77
B386-G322	15.55	0.90	−1.09	−1.04	61.67	−4.30	14.08
B514	15.76		−2.06	−2.12	−242.32	−15.11	55.30

Note. [a] [Fe/H] values are on the Zinn & West (1984) metallicity scale and were transformed to the new scale defined by Carretta et al. (2009) ([Fe/H]$_{C09}$) using the linear transformation provided in that paper.

With this paper we turn our interest to the other large spiral in the Local Group, the Andromeda galaxy (M31). The systematic study of the variable star population in M31 is fairly recent. Indeed, at a distance of 752 kpc ± 27 (Riess et al. 2012), at least 4-m telescopes (see, e.g., Pritchet & van den Bergh 1987) and preferably 8 m-class telescopes are needed to resolve and measure individual stars in the field of Andromeda from the ground, while only the resolution capabilities of the *Hubble Space Telescope* (*HST*) allow to resolve individual stars on different evolutionary paths, including the RRL stars, in GCs or crowded fields in Andromeda. Only five "classical" dSph satellites of M31 have been analyzed for variability so far (And VI: Pritzl et al. 2002; And II: Pritzl et al. 2004; And I and III: Pritzl et al. 2005; and And V: Mancone & Sarajedini 2008) and, unlike the MW dSphs, all three Oosterhoff types (Oo I, Oo II, and Oo-Int) were observed. As far as the field of M31 is concerned, our current knowledge relies on a few relatively recent studies which have provided a detailed analysis of more than a thousand RRL stars in the M31 field. Different components of M31 were analyzed, e.g., halo, disk, stream (Brown et al. 2004; Jeffery et al. 2011) including regions close to M32 (Sarajedini et al. 2009; Fiorentino et al. 2010b, 2012; Sarajedini et al. 2012), and all these studies agree on the M31 field variables having properties consistent with an Oosterhoff type I classification. For the study of the Oosterhoff dichotomy, however, cluster RRL stars are needed. A pioneering study of the RRL stars in four M31 GCs was presented by Clementini et al. (2001), who detected a number of RRL candidates in the M31 clusters G11, G33, G64, and G322, based on $F555W$, $F814W$ *HST* Wide Field Planetary Camera 2 (WFPC2) archive observations. However, the number of phase points and the time window of these archive data were too sparse to allow the derivation of the variable stars' periods. Thus, we do not know yet whether the M31 GCs show the Oosterhoff dichotomy, or whether indeed they can be placed into an Oosterhoff type at all.

WFPC2 observing time to study the RRL stars in six M31 GCs was granted to us in *HST* Cycle 15, under program GO 11081 (PI: G. Clementini). We obtained time-series photometry for G11, G33, G76, G105, G322, and B514 for which the basic parameters are reported in Table 1. These M31 GCs have well-defined color–magnitude diagrams (CMDs; Rich et al. 2005; Galleti et al. 2009), metallicities compatible with the existence of RRL stars, as well as populous horizontal branches (HBs) stretching across the instability strip (IS), hence providing a good probability of having RRL stars. Three of these GCs—G76, G105, and G322—have a metallicity that, in the MW, would place them in the Oo I group, whereas the other three—G11, G33, and B514—are more metal-poor and, in the MW, would be expected to be Oo II GCs. Figure 1 shows
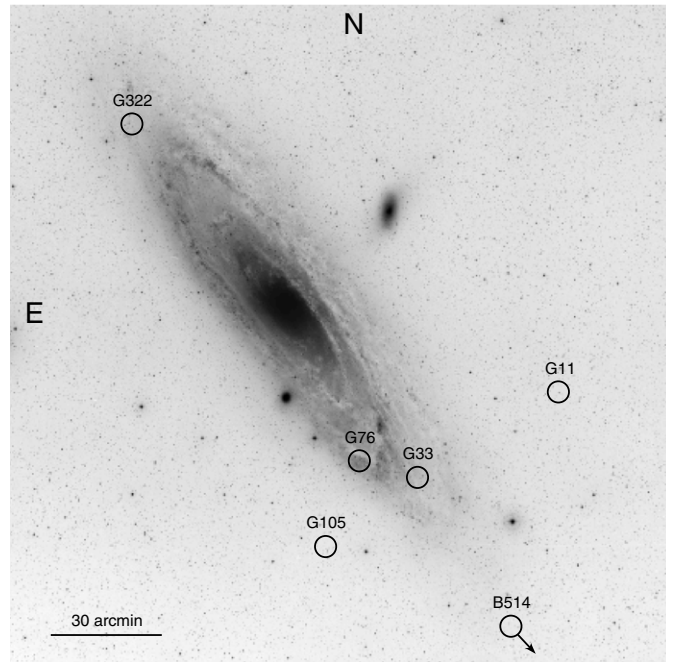

Figure 1. Location of the GCs targeted in the Cycle 15 *HST* program GO 11081 on a ∼2.9 × 2.9 deg² POSSI/O/DSS2 image of the Andromeda galaxy from the Digitized Sky Survey available at CDS (Strasbourg). Clusters G11, G105, and B514 are located in the M31 halo, whereas G76, G33 and G322 are projected on the disk component of M31. B514 is the farthest GC in our sample at a distance of ∼4 deg from the center of M31, and its real position does not appear in this map.

the positions of these six GCs on a ∼2.9 × 2.9 deg² image of M31. They span distances in the range of ∼45 arcmin (G76) to ∼4 deg (B514) from the center of M31, thus allowing us to probe different areas of Andromeda, from the galaxy's unperturbed halo to regions close to the giant stream. We are aware that these few clusters may not necessarily be representative of the entire GC ensemble of M31, still they allowed us to check for the first time whether the properties of the RRL stars in the M31 GCs are compatible with the Oosterhoff dichotomy, and whether they show the same correlations with HB morphology as seen in the MW. It is worth noting that the presence of the Oosterhoff dichotomy in the MW GC system was first established on the basis of a study of the RRL properties in only five MW clusters, of which three turned out to be of Oosterhoff type II, and two of Oosterhoff type I. A first characterization of the variable stars of B514 based on this data set was published by Clementini et al. (2009), who detected and derived periods for 89 RRL stars (82 RRab and 7 RRc pulsators) among 161 candidate variables identified in the cluster. The average period of the RR Lyrae variables, and the position in the period–amplitude diagram both suggested for B514 an Oo I classification, in spite of its low metallicity ([Fe/H] = −2.06, Galleti et al. 2009). A preliminary study of the other five M31 GCs has been presented in Contreras Ramos (2010).

In this paper we present results from the detailed study of the variable star population in G11 (Bo293) based both on our Cycle 15 observations and on the *HST* archival data analyzed by Clementini et al. (2001). We also describe in detail the overall strategy we have applied to characterize the variable star population in all the M31 GCs we observed in Cycle 15. The results for these other M31 GCs will be presented in two forthcoming papers.

G11 (Bo293; R.A.(J2000) = $00^h36^m20^s.86$, decl.(J2000) = $40°53'37''.25$), is a relatively massive ($M_V \approx -8.5$ mag) GC,

Table 2
Log of the Observations

Dates	HJD Interval (−2450000) (days)	Filter	Exposure Length (s)	N	Total Exposure (s)
2000 Feb 3	1577.73–1577.82	F555W	1200/1300/2 × 1400	4	5300
2000 Feb 3	1577.86–1577.95	F814W	2 × 1300/2 × 1400	4	5400
2007 Jul 30–31	4312.16–4312.82	F606W	1100	11	12100
2007 Jul 30–31	4312.18–4312.84	F814W	1100	11	12100

at a projected distance of ∼75.75 arcmin from the center of M31 (Revised Bologna Catalog (RBCV4.0); Galleti et al. 2004[10]). According to its spatial location the main source of contamination for G11 is expected to come from the M31 halo population, whereas the contribution by disk stars is expected to be lower than 10% (Bellazzini et al. 2003). The metal abundance of G11 has been calculated both photometrically (see, e.g., Bonoli et al. 1987; Fan et al. 2010) and with integrated spectroscopy (see, e.g., Huchra et al. 1991; Galleti et al. 2009) and all results agree on a moderately low amount of metals. In the following we have adopted the most recent spectroscopic re-evaluation of the cluster metallicity by Galleti et al. (2009): $[Fe/H]_{ZW} = −1.59 \pm 0.23$ and $[Fe/H]_{C09} = −1.60 \pm 0.24$ (on the Zinn & West 1984, and the Carretta et al. 2009 metallicity scales, respectively). Rich et al. (2005) and Federici et al. (2012) estimated a reddening $E(B − V) = 0.10$ mag and 0.12 mag, respectively, on the line of sight of G11, and characterized the cluster as having a blue HB morphology.

We present in Section 2 the WFPC2 data used in our analysis. In Sections 3 and 4, we discuss the method used to reduce the time-series photometry, to detect the variable stars, and to derive their periodicities. In Section 5, we present the RRL sample and the cluster's CMD together with the Oo classification and the distance modulus of G11. Finally in Section 6 we summarize our main results.

2. OBSERVATIONS

WFPC2 time-series observations of G11 were obtained on 2007 July, as part of the Cycle 15, *HST* GO program 11081 (PI: G. Clementini). They consist of 11 *F*606*W* (broad *V*) and 11 *F*814*W* (*I*) exposures each of 1100 s in length, taken by alternating the two filters. This filter selection allows our data to be directly comparable with most previous *HST*-based studies of GCs and field stellar populations in the MW and in M31, including the M31 field RRL stars studied by Brown et al. (2004), Sarajedini et al. (2009), and Jeffery et al. (2011). The exposure length of our observations was the best compromise to achieve reasonably good signal-to-noise ratio (S/N) even for measurements corresponding to the minimum light of the M31 RRL stars ($V \sim 25.5$–25.7 mag), and, at the same time, to avoid smearing the light curves. These were also the longest possible exposures allowing us to fit an *F*606*W*, *F*814*W* pair of images into one orbit. The observations were scheduled in one 11-orbit block with a 50 minute gap between each pair of observations, for a total exposure time on target of 3 hr and 22 minutes in each band, distributed over a total time-window of ∼16 consecutive hours. The cluster was roughly centered on the planetary camera (PC) of the WFPC2, which provides better spatial resolution ($0''.046$ pixel^{-1}), while the lower resolution ($\sim 0''.1$ pixel^{-1}) wide-field cameras sampled the surrounding M31 halo field. The

WFPC2 has a total field of view (FOV) of $150'' \times 150''$, which corresponds to a projected area of 0.6×0.6 kpc^2 at the distance of M31. The tidal radius (r_t) estimated for G11 is ∼16 arcsec (Clementini et al. 2001), hence, the region inside the cluster tidal radius is entirely contained in the PC camera ($34'' \times 34''$). Our proprietary data were complemented by WFPC2/*HST* archive observations of G11 obtained in 2000 as part of the GO program 6671 (PI: Rich). They consist of four *F*555*W* (*V*) and four *F*814*W* (*I*) frames. The individual exposures of the archival data are about 20 minutes long, and were taken consecutively over a total time interval of 5 hr and 15 minutes. A log of both the proprietary and archival observations of G11 used in the present study is provided in Table 2.

3. DATA REDUCTION

Point-spread function (PSF) photometry of the individual pre-reduced images of G11 supplied by the STScI pipeline was performed with HSTphot (Dolphin 2000), a photometry package specifically designed to handle the undersampled PSF of the WFPC2/*HST* data. A number of initial pre-processing steps are required before running the photometry procedure. First, image defects such as bad columns and saturated pixels are identified using the information provided in the data quality files. They are then masked by setting them to the bad data value, −100 ADU, and are ignored afterward. Next, cosmic rays and hot pixels are flagged automatically and sky images are created in order to provide an initial guess of the background. At the same time, the *X, Y* offsets between each image and a reference image (for G11 the image u9x6f001m_c0f in the *HST* archive, see http://archive.stsci.edu/) are measured using the IMEXAMINE task in IRAF. These offsets are input into the multi-photometry mode of HSTphot in order to measure the magnitudes of the objects detected in each image. The photometric measurements were performed using PSFs employing the "weighted PSF fitting mode," which places more weight on the central part of the star profile and less on the outer pixels. The photometric procedure automatically applies aperture and charge transfer efficiency corrections and transforms the instrumental magnitudes to the *HST* flight-photometric system as well as to the Johnson–Cousins system, using the transformations available at http://purcell.as.arizona.edu/wfpc2_calib/, that are based on the calibration formulas by Holtzman et al. (1995). In addition to position, magnitudes and errors, HSTphot provides in the output photometry file a variety of quality information for each detected source, namely, the "object type" (stellar, extended, bad star, etc.), the χ^2, which simply gives the quality of the PSF fit, the "sharpness" used to eliminate cosmic rays and extended objects, the "roundness," the S/N, and a "crowding" parameter that describes the change in star brightness if neighbors are not subtracted. We used the aforementioned quality information to clean the list of detected sources, keeping for the following analysis only stellar detections with valid photometry
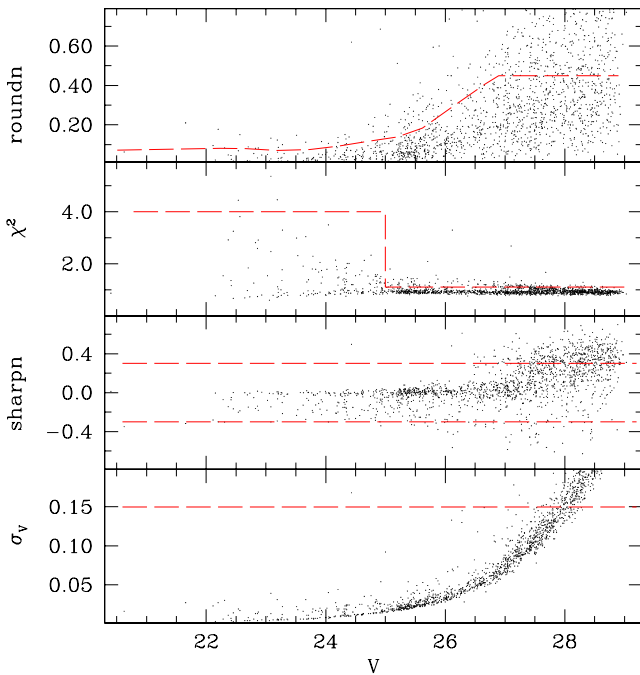
Figure 2. HSTphot quality image parameters of the G11 data for the PC. The dashed lines show the cuts we have applied to the photometric catalogs.

(A color version of this figure is available in the online journal.)

Figure 3. V, $V - I$ CMD of the stellar sources (object type flag=1) in the FOV of the Cycle 15 observations of G11, selected as described in Section 3. Circles and triangles mark, respectively, fundamental-mode (RRab) and first-overtone (RRc) RRL stars we have identified in the whole FOV of the G11 observations, with filled and open symbols corresponding to variable stars within and outside the cluster tidal radius, respectively (see the text for details).

(A color version of this figure is available in the online journal.)

(object type flag=1) on all input images, global sharpness parameter $-0.3 \leqslant \text{sharpness} \leqslant 0.3$, $\chi^2 \leqslant 1.1$ if $V > 25.0$ mag and $\chi^2 \leqslant 4.0$ if $V < 25.0$ mag, roundness $\leqslant 2 \times \langle \text{roundness} \rangle$ and in any case less than 0.45, and $\sigma_V, \sigma_I < 0.15$ mag. Figure 2 shows the cuts applied to the data of the PC. The V, $V - I$ CMD of all sources satisfying these conditions in our Cycle 15 observations of G11 is presented in Figure 3. The limiting magnitudes of our photometry, defined as a 4 σ detection, are $V \sim 27.5$ mag in all four cameras, and $I \sim 26.7$ mag and 27 mag on the PC and the WF cameras, respectively. The internal photometric errors in V magnitude and $V - I$ color provided by HSTphot are of ~ 0.01 mag down to $V \simeq 24$ mag; then increase continuously up to ~ 0.1 and 0.18 mag, respectively, from $V \simeq 24$ mag to 27.5 mag. At the level of the HB ($V \simeq 25$ mag) the photometric errors are typically of ~ 0.02 mag in V, and ~ 0.04 mag in $V - I$.

4. IDENTIFICATION OF THE VARIABLE STARS AND PERIOD SEARCH

The identification of the G11 variable stars was based exclusively on the Cycle 15 observations. The archive data were used, when possible, only for the purpose of improving the period definition and the calibration process. Identification of the variable stars was carried out using two different approaches. First, candidate variables were identified from the scatter diagrams of the $F606W$ and $F814W$ data sets, using VARFIND, custom software developed at the Bologna Observatory by P. Montegriffo. Briefly, VARFIND computes the standard deviation of the mean magnitude of each source over the entire set of individual measurements and compares the standard deviation with the mean magnitude (scatter diagram). Variable stars show larger standard deviations than constant stars due to the light variation. Fainter stars will also have larger standard deviations due to the photon noise, so it is advisable to proceed with caution at low luminosity levels.

Our second approach was to compute for each measured source a revised version of the variability index (Welch &
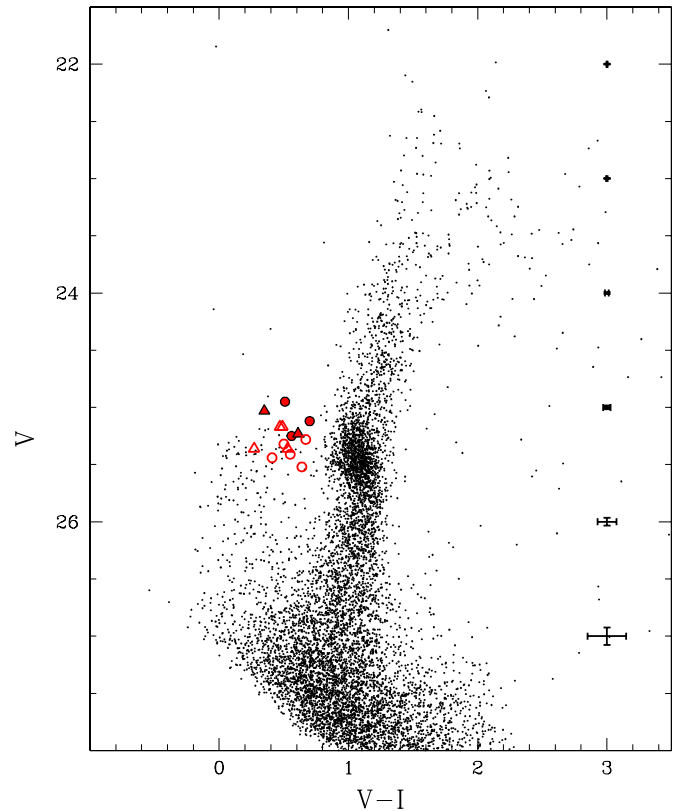
Stetson 1993; see also Stetson 1996 for a detailed definition and description), specifically adapted to the HSTphot photometry of the G11 time-series. Basically, for each star the residual of each individual magnitude measurement with respect to the weighted mean magnitude in each photometric band is calculated and normalized by the photometric error ($R = (x - \bar{x})/\text{err}$). Then, residuals corresponding to pairs of V and I observations closely spaced in time are multiplied and finally added ($\sum_{i=1}^{n}(R_{V_i} * R_{I_i})$). If a star is a genuine variable, it will be brighter than usual in V when it is also brighter than usual in I, and vice versa. Therefore, the total sum of the residual-products will be positive. On the other hand, if the star is constant, and there are only small random errors in its magnitudes, then the V-band and I-band residuals will be uncorrelated and should have the same sign half the time, and opposite sign the remaining half, leaving the overall sum of the residual product close to zero.

The light curves of the candidate variables found with the above procedures were then inspected visually. Period search and study of the light curves were performed using two different methods. A first verification of variability and guess of the star periodicity was obtained using the phase dispersion minimization (PDM) algorithm (Stellingwerf 1978) in the IRAF environment. PDM is a generalization of the Lafler & Kinman (1965) algorithm, and essentially attempts to identify the phased light curve that produces the minimum scatter in phase. The period refinement was then obtained with the Graphical Analyser of Time Series (GRATIS), private software developed at the Bologna Observatory by P. Montegriffo (see,
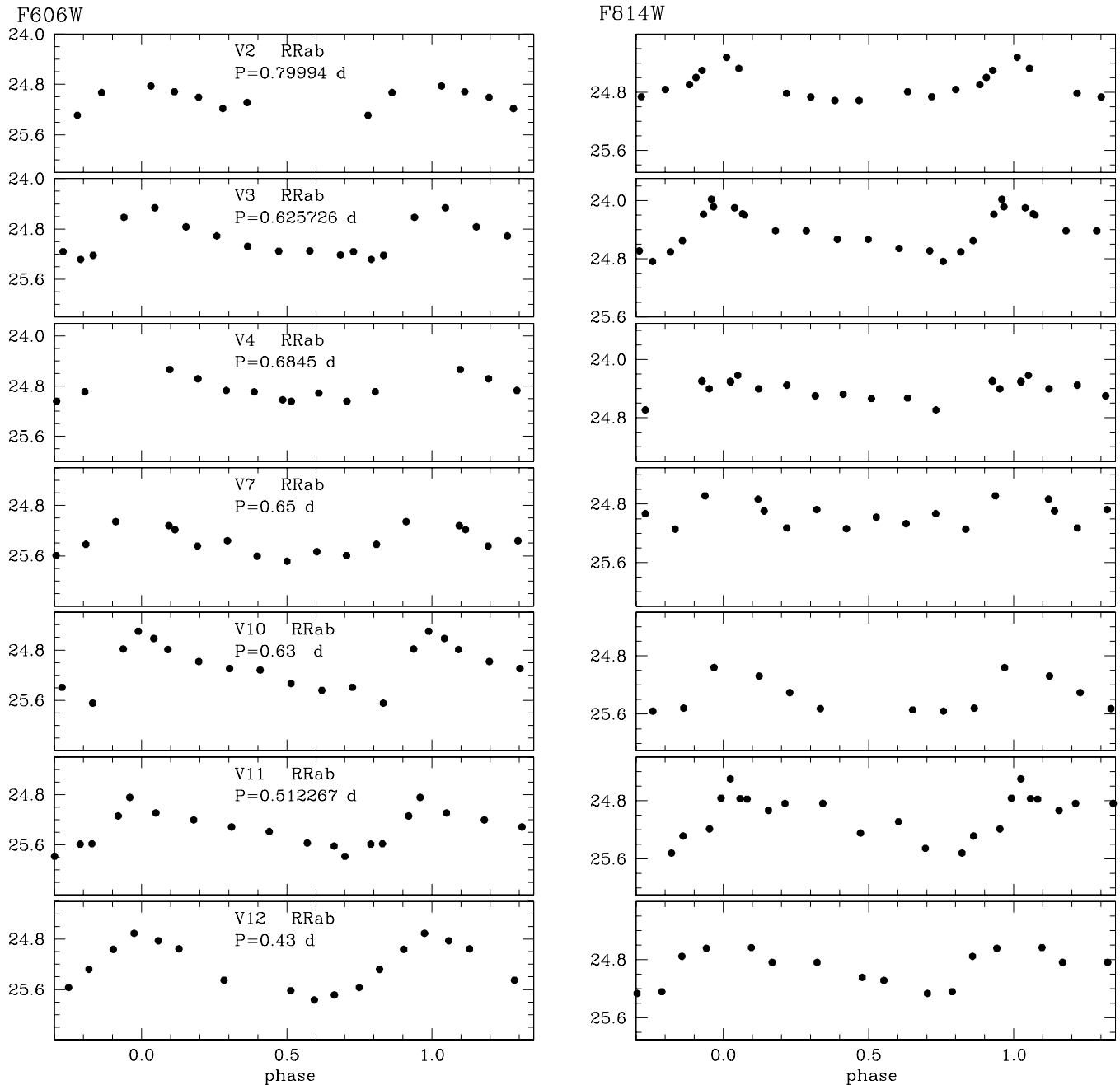
Figure 4. $F606W$, $F814W$ light curves of the RRL stars detected in this study, ordered by increasing distance from the cluster center (R.A. (2000) = $00^h36^m20^s.86$; decl.(J2000) = $40°53'37''.25$). Typical errors of the single data points are of about 0.08 mag and 0.13 mag in $F606W$ and $F814W$, respectively.

e.g., Clementini et al. 2000), which uses both the Lomb periodogram (Lomb 1976) and the best fit of the data with a truncated Fourier series (Barning 1963). We confirmed the variability, and obtained reliable periods and light curves for 14 candidate variables. Because of the relatively short-time interval spanned by the Cycle 15 observations, our periods are generally accurate to two/three significant figures. However, six of the confirmed variable stars have a counterpart in the photometric catalog of the 1999–2000 observations. For these variables we directly combined the Cycle 15 and the archival $F814W$ data sets. The long gap between the two data sets did not cause significant aliasing difficulties in phasing the $F814W$ data, whereas there were problems to phase the archive $F555W$ and the $F606W$ data, but this was mainly due to the different passbands covered by these filters. The $F606W$ and $F555W$

data were thus used separately to iterate the period search procedure. In turn periods accurate to five/six significant figures were obtained for the stars with both proprietary and archive time-series (see the next section).

5. RESULTS

5.1. The RR Lyrae Stars

The 14 variable stars identified in the FOV of the G11 observations are of RR Lyrae type, and include eight fundamental-mode and six first-overtone pulsators. The light curves of the variables in the $F606W$ and $F814W$ filters are presented in Figure 4. They are well sampled in both bands. The identification, basic elements and photometric properties of the confirmed RRL stars in our study are provided in Table 3. The variable
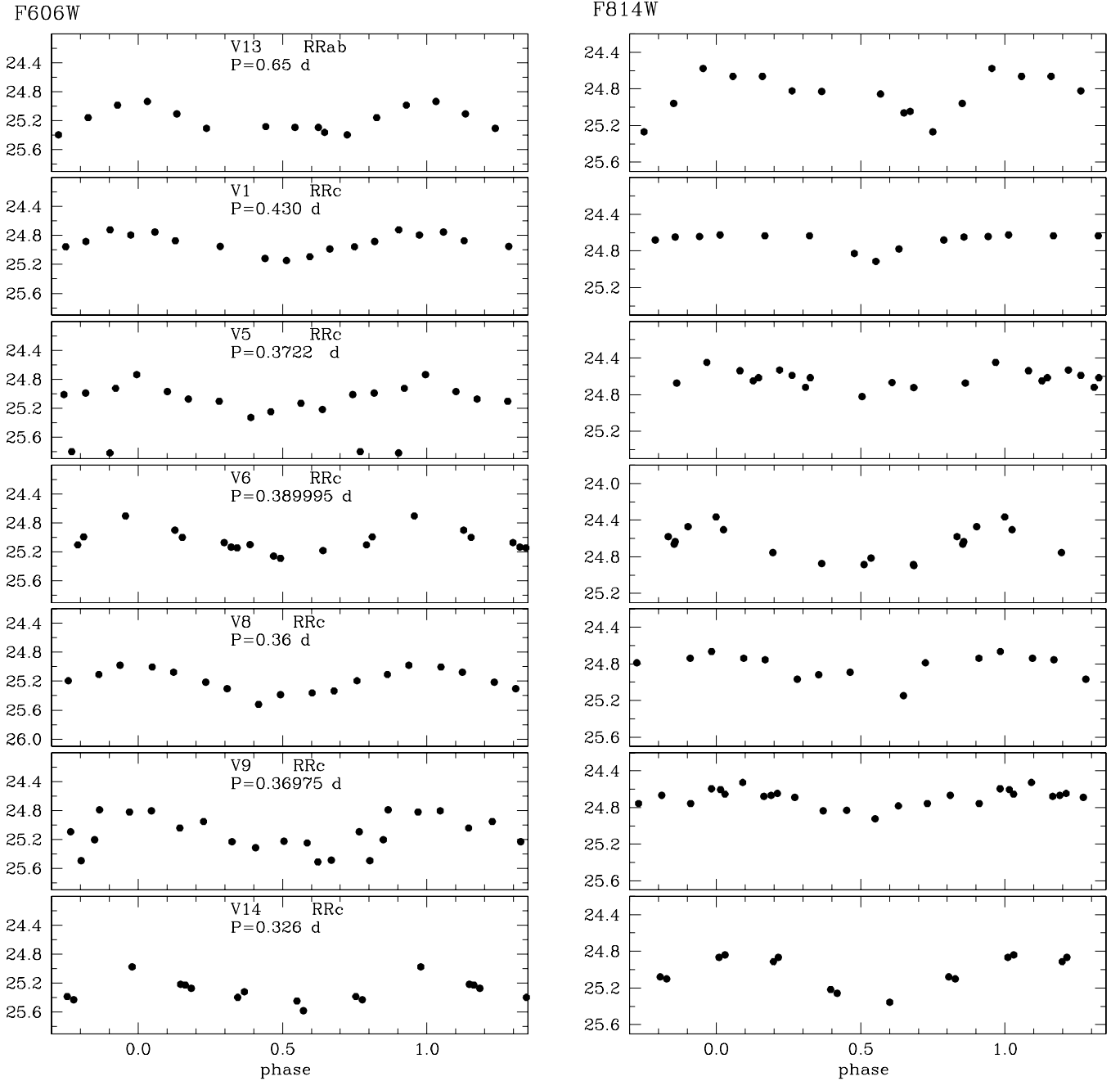
Figure 4. (Continued)

stars are ordered by increasing distance from the center of G11. Column 1 indicates the star's ID. Column 2 indicates the camera of the WFPC2 where the star is located. Columns 3 and 4 provide the star's coordinates in pixels, as measured on the reference image (see Section 3). Column 5 gives an estimate of the distance from the cluster center, whereas Columns 6, 7, and 8 give the RRL type, the star's period, and the Heliocentric Julian date of maximum light. Columns 9 and 10 give the intensity-averaged mean $F606W$ and $F814W$ magnitude values, while Columns 11 and 12 list the corresponding $F606W$ and $F814W$ amplitudes of the light variation, Columns 13 and 14 give the intensity-averaged mean V and I magnitudes, and Columns 15 and 16 list the corresponding A_V and A_I amplitudes. Clementini et al. (2001) identified two candidate RRL stars in G11, based

on the 2000 data set. We confirm the variability of one of the Clementini et al. (2001) candidates that in fact corresponds to the RRc star V5 in the present study.

The time-series photometry of the variable stars in the $F606W$, $F814W$ *HST* flight-system is provided in Table 4, which is published in its entirety in the online journal. A map showing the position of the RRL stars detected in the whole $\sim2.6 \times 2.6$ arcmin^2 FOV covered by the WFPC2 observations of G11 is presented in Figure 5, where we have drawn on the PC a large open circle with the cluster tidal radius. RRL stars falling inside this region are marked by filled circles and triangles for RRab and RRc stars, respectively, while variable stars outside this region were marked with the corresponding open symbols. In the figure the three circular regions marked as I, II, and III on

Table 3
Identification and Properties of the RRL Stars Identified in the FOV of the G11 Observations

Name	Camera	x (pixel)	y (pixel)	Dist. (arcsec)	Type	P (days)	Epoch (max) (-2450000)	$\langle F606W \rangle$ (mag)	$\langle F814W \rangle$ (mag)	A_{F606W} (mag)	A_{F814W} (mag)	$\langle V \rangle$ (mag)	$\langle I \rangle$ (mag)	A_V (mag)	A_I (mag)
							Variable stars within the cluster tidal radius								
V1	PC	346.11	428.77	2.76	RRc	0.43	4312.37	24.93	24.70	0.36	0.24	25.03	24.68	0.42	0.27
V2[a,b]	PC	414.70	370.00	2.88	RRab	0.79994	1577.940	25.11::	24.73	$\geqslant 0.54$	0.60	25.25::	24.69	$\geqslant 0.62$	0.54
V3[a]	PC	466.85	400.35	3.16	RRab	0.625726	1576.656	24.93	24.45	0.86	0.78	25.12	24.42	0.91	0.77
V4[a]	PC	335.19	434.09	3.26	RRab	0.6845	1577.915	24.80	24.46	0.53	0.39	24.95	24.44	0.64	0.38
V5[a,c]	PC	267.53	514.53	7.42	RRc	0.3722	4312.760	25.06	24.65	0.40	0.21	25.23	24.62	0.49	0.20
							Variable stars beyond the cluster tidal radius								
V6[a]	PC	84.04	643.00	17.71	RRc	0.389995	4312.2425	25.02	24.72	0.64	0.47	25.17	24.68	0.49	0.44
V7	PC	751.29	234.25	18.30	RRab	0.65	4312.750	25.34	24.90	0.84	0.57	25.52	24.88	0.97	0.68
V8	WF4	310.58	97.27	45.00	RRc	0.36	4312.248	25.21	24.85	0.45	0.32	25.36	24.83	0.51	0.31
V9[a]	WF2	532.38	381.04	60.52	RRc	0.36975	4312.172	25.05	24.73	0.49	0.25	25.17	24.70	0.58	0.26
V10	WF2	448.81	454.15	63.50	RRab	0.63	4312.168	25.10	24.65	1.15	0.79	25.28	24.61	1.39	0.70
V11[a]	WF2	762.01	235.43	65.48	RRab	0.51226	1577.340	25.31	25.05	1.01	0.84	25.44	25.03	1.20	0.85
V12	WF2	535.71	445.34	66.27	RRab	0.43	4312.37	25.26	24.89	1.01	0.76	25.41	24.86	1.15	0.75
V13[b]	WF4	518.17	708.96	80.43	RRab	0.65	4312.405	25.20	24.83	0.45	0.67	25.32	24.82	0.43	0.68
V14	WF3	647.69	482.84	98.74	RRc	0.326	4312.765	25.28	25.10	0.60	0.49	25.36	25.09	0.65	0.49

Notes.
[a] Stars with a counterpart in the archival WFPC2/*HST* data.
[b] Stars showing blue amplitudes (A_{F606W} or A_V) smaller than the red amplitudes (A_{F814W} or A_I), possibly due to contamination by companions.
[c] Candidate RRL star in Clementini et al. (2001) that has been confirmed in the present study.

Table 4
$F606W$, $F814W$ Photometry for the RRL Stars Detected in the FOV of the G11 Observations

G11 - Star V1 - RRab			
HJD (-2454312)	$F606W$ (mag)	HJD (-2454312)	$F814W$ (mag)
0.160941	24.83	0.177609	24.47
0.225529	24.92	0.242197	25.03
0.292201	25.01	0.308869	24.81
0.358873	25.19	0.375541	24.86
0.425545	25.09	0.442213	24.91
0.492217	24.91	0.508885	24.91
0.558889	24.87	0.575557	24.52
0.625561	24.97	0.642229	24.79
0.692233	25.03	0.708901	24.86
0.758211	25.29	0.774879	24.76
0.824883	24.93	0.841551	24.69

(This table is available in its entirety in a machine-readable form in the online journal. A portion is shown here for guidance regarding its form and content).

the WF cameras enclose the same area contained in the cluster's tidal radius on the PC, and were used to check the contamination by field stars of the cluster CMD (see Section 5.2). Figure 6 provides the finding chart of the seven variables detected on the PC.

In order to plot the variable stars in the CMD and in the period–amplitude diagram we have converted the *HST* flight-system magnitudes into the Johnson–Cousins photometric system. The calibration of the $F606W$, $F814W$ light curves to the Johnson–Cousins V, I was performed through a procedure that properly takes into account the variation in color of the variable stars during the pulsation cycle. This procedure, which we developed and widely tested in a number of other studies (see, e.g., Baldacci et al. 2005; Fiorentino et al. 2010a for previous applications with ground-based and *HST* data, respectively) basically performs the following steps: (1) to each single phase
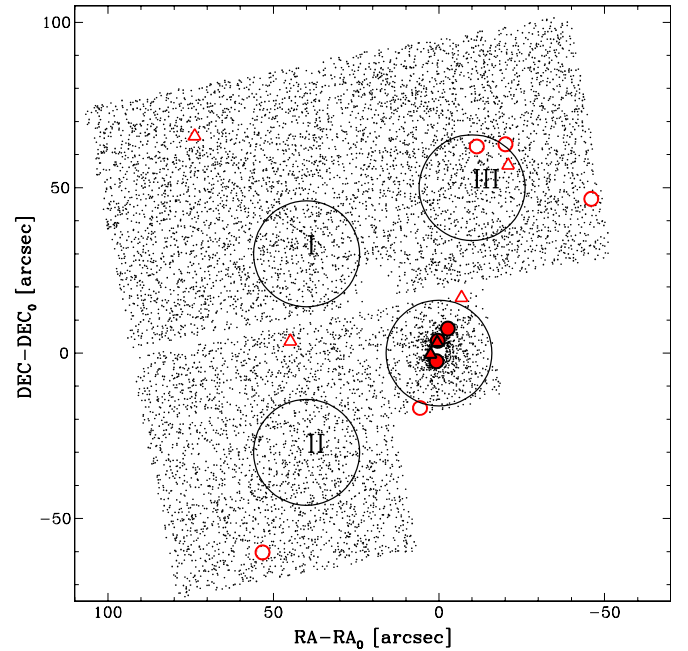

Figure 5. Map of the stellar sources in the $\sim 2.6 \times 2.6$ FOV covered by the WFPC2 observations of G11. Black points mark non-variable sources. RRab and RRc stars are marked by circles and triangles, respectively. Filled (red) symbols indicate the likely cluster members, whereas empty symbols indicate RRL stars outside the cluster tidal radius. The large empty circles on the four cameras of the WFPC2 are drawn with the tidal radius of G11 as derived by Clementini et al. (2001).
(A color version of this figure is available in the online journal.)

point in a given filter associates the color at the corresponding proper phase read from the Fourier models best fitting the star light curves[11] obtained with the GRATIS package; (2)

---

[11] Depending on the sampling of the light curves, from one up to three harmonics were used to fit the RRc light curves, whereas from two up to five harmonics were used the RRab stars.
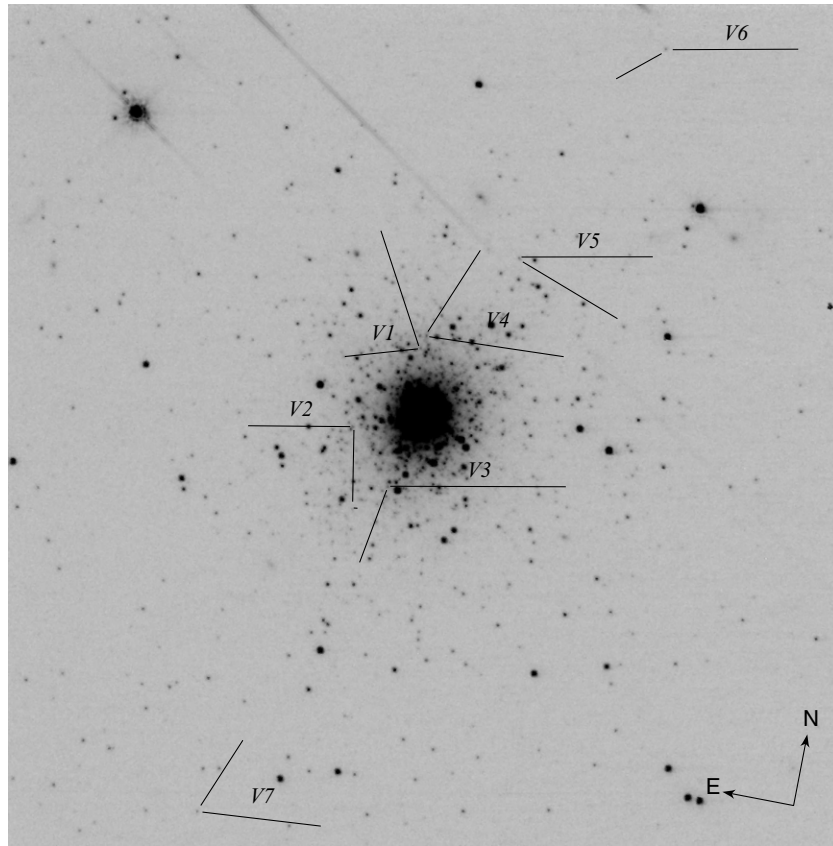
Figure 6. Finding chart of the seven variable stars identified on the $34'' \times 34''$ FOV of the PC.

this color is then entered into the calibration equations (in the present case Holtzman et al. 1995 equations), thus obtaining individual V, I calibrated data. The V, I-calibrated light curves are then reanalyzed with GRATIS (by imposing the final period, epoch of maximum light and optimal number of harmonics defined during the period search process) in order to compute the intensity-averaged mean magnitudes and the amplitudes listed in Table 3. We explicitly note that, although HSTphot provides mean magnitudes of all photometrized stars in the Johnson–Cousins system, these values are not appropriate for variable stars for two reasons: (1) for variable stars the mean magnitude strictly depends on the sampling of the light curve, making it necessary to use models/templates in case of poor sampling; (2) HSTphot provides mean magnitudes computed as the average of the magnitude values, however, intensity-averaged mean magnitudes are needed for the variable stars, since this is the kind of mean value that better approximates the luminosity the variable star would have were it non variable (see, e.g., Caputo et al. 2000). The 14 confirmed variable stars are plotted in the CMD, using their intensity-averaged mean magnitudes and colors, and filled/open circles and triangles for RRab and RRc stars within/outside the cluster tidal radius, respectively. According to Figure 5, 7 of the 14 RRL stars fall inside the PC FOV, 5 being within the cluster tidal radius and 2 (V6 and V7) located slightly outside r_t. The position in the CMD of these two variables suggests that V6 is likely a cluster member, while V7 lies slightly below the cluster HB and could possibly be a background interloper. To be conservative, in the following we will consider also V6 as a field star, however we note that including the star in the cluster RRL sample would not affect the results of our analysis. The remaining seven RRL stars are placed in more external regions and may in part belong to the

M31 halo (see Section 5.3). Although the number of RRL stars found within the cluster tidal radius is fairly small, this result is consistent with the rather blue HB morphology exhibited by G11 (see Figure 11 in Rich et al. 2005, recall that predominantly blue HB clusters often contain few, if any, RRL variables), and it is also consistent with the Clementini et al. (2001) results.

5.2. Color–Magnitude Diagram

In Figure 7 we have divided the stars in the CMD of Figure 3 in three regions at increasing distance from the center of G11, in order to better isolate the cluster stars from the M31 field population. The left panel of the figure corresponds to the region within the tidal radius of G11. The CMD of this region shows two evolutionary sequences that clearly trace the cluster stars: (1) a rather steep red giant branch (RGB), indicating that G11 is relatively metal poor, in agreement with the metallicity values found in the literature (Rich et al. 2005; Galleti et al. 2009; Federici et al. 2012); and (2) an extended blue HB, which is absent in the control field shown in the central panel of Figure 7. To check whether these extremely blue stars do indeed belong to the G11 HB, in Figure 8 we compare the CMD of the stars within the cluster tidal radius on the PC with the CMDs of stars located in the three equal-area external regions of the WF cameras shown in Figure 5. The number of extremely blue stars is significantly larger in the region within the G11 tidal radius (9) than in field I (2), II (1), and III (1; see Figure 8), thus confirming that these stars likely belong to the G11's HB. These two features, along with the mere presence of RRL stars, lead to conclude that G11 is older than 10 Gyr and most likely of Oo II type, as confirmed by the mean period of its RRab variables (see Section 5.3).
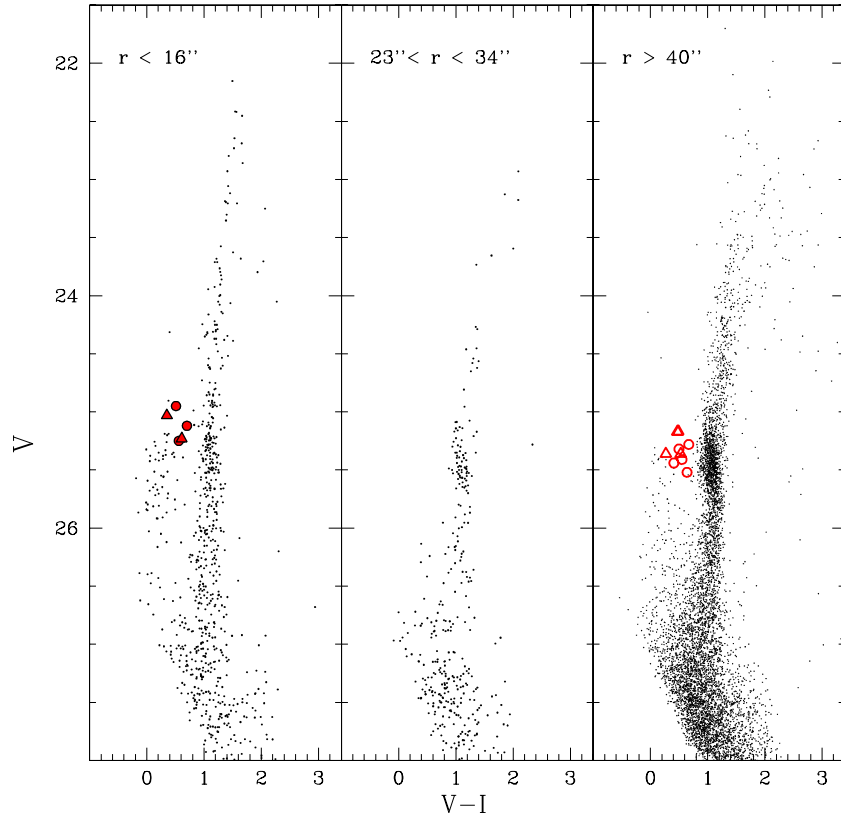
Figure 7. V, $V - I$ CMD of the sources located in three regions with increasing the distance from the cluster center. The adopted distances from the cluster center are indicated in the panels. Symbols and color-coding are the same as in Figures 3 and 5.

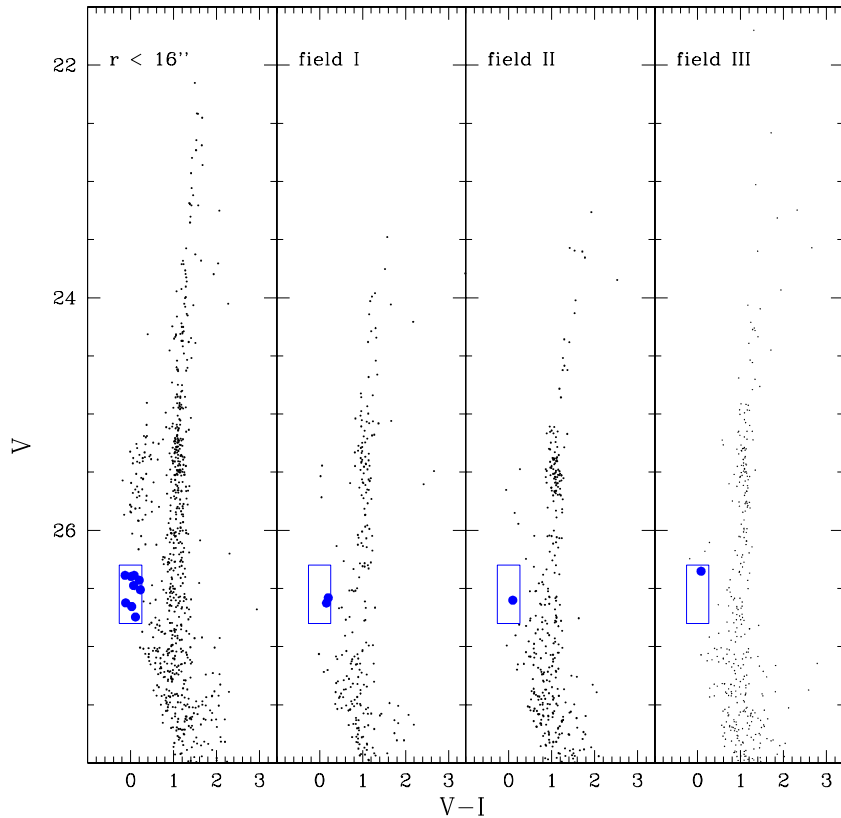(A color version of this figure is available in the online journal.)

Figure 8. V, $V - I$ CMDs of the four regions of equal area shown in Figure 5, that were drawn with the tidal radius of G11. We have marked with (blue) filled circles and encircled with boxes stars with $26.3 \leqslant V \leqslant 26.8$ mag and $V - I \lesssim 0.2$ mag that belong to the extreme blue HB of G11 (see the text for details).

(A color version of this figure is available in the online journal.)
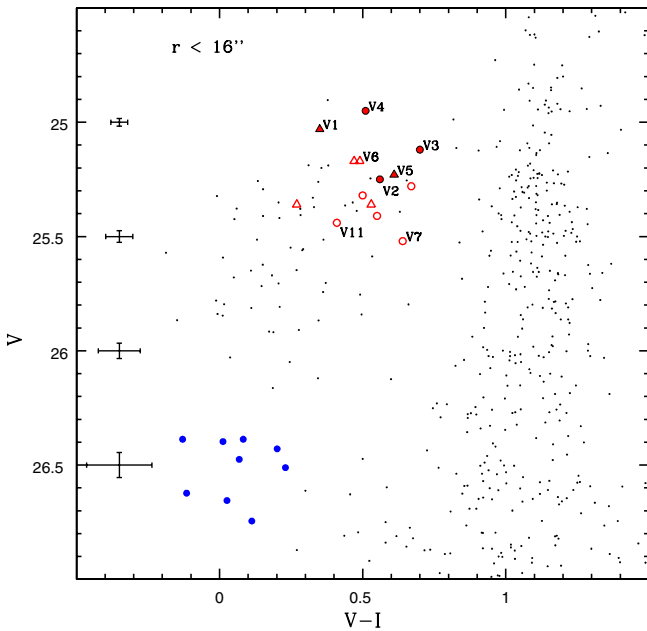
Figure 9. Blow-up on the HB for stars within 16″ from G11 center. Overplotted are the RRL stars within (filled symbols) and outside (open symbols) the cluster tidal radius. Symbols and color-coding are the same as in Figures 3 and 5. Marked with (blue) filled circles are stars belonging to the extreme blue HB of G11.

(A color version of this figure is available in the online journal.)

The middle panel of Figure 7 shows an intermediate region of our FOV, whose limits were chosen in order to enclose the same area covered by the G11 tidal radius and thus easily estimate the field contribution to the cluster CMD. The field contamination does not appear to be a significant issue, being negligible at the HB level. No RRL stars have been found in this region.

Finally, in the right panel of the figure, we show the outermost region of our FOV, which better traces the M31 halo stellar population. In fact, we can clearly see some well-known features of M31: a broad RGB with a descending tip, and an extended red clump located at $V \sim 25.0$–25.5 mag and $V - I \sim 1$ mag. We can also easily distinguish a minor sign of blue stars (with color $\lesssim 0.5$ mag), which may be the contribution of main-sequence intermediate-age stars (blue plume) possibly associated with the galaxy disk, and/or blue HB stars belonging to the old field population associated with the galaxy's halo. An old population (older than 10 Gyr) is confirmed by the seven RRL stars we have identified in this region. Figure 9 shows an expanded view of the HB: Field and cluster variables fall reasonably well in the appropriate region of the HB according to their pulsation modes and colors. The only exceptions are the RRab star V4 and the RRc star V5 among the cluster variables, which are respectively slightly too blue and too red for their pulsation modes, and the field RRab star V11, which is slightly too blue. We note also that V4 and V1 are about 0.1–0.2 mag brighter than all the other cluster variables. We suspect that they might be contaminated by unresolved companions. On the other hand, the field RRab star V7 is slightly fainter than all the other variables, suggesting that it might be a background object. Figure 9 also shows that a number of objects lying inside the IS region do not show any RRL-like variation. We believe that these objects are the result of blending in the dense core region, mainly between blue HB stars and red giants (see Rich et al. 2005, for a detailed discussion of this effect). Another possibility is also that they are back/foreground field stars.

5.3. The Oosterhoff Type of G11

The average period of the three RRab stars located within the G11 tidal radius is $\langle P_{ab} \rangle = 0.70$ days ($\sigma = 0.09$ days, average on three stars), suggesting a classification of G11 as Oo type II. Similarly, the average period of the two RRc stars: $\langle P_c \rangle = 0.40$ days ($\sigma = 0.04$ days, average on two stars), and the fraction of c-type RR Lyrae, $f_c = 0.4$, are also consistent with an Oo II classification (see Section 1). However, Catelan et al. (2012) note that neither $\langle P_c \rangle$ nor f_c appear to be good Oosterhoff indicators and suggest that $P_{ab,\text{min}}$, besides $\langle P_{ab} \rangle$, is a quantity that better defines the Oosterhoff status of a stellar system. In the case of G11, the shortest-period RRab (within the cluster tidal radius) is star V3 with $P_{ab,\text{min}} = 0.626$ days, which also suggests an Oo II classification, albeit within the limits of poor statistical significance.

In Figure 10, we show the run of $\langle P_{ab} \rangle$ values vs. metallicity for the GGCs containing RRL stars, using for the clusters' metallicity the Zinn & West (1984) scale in the left panel, and the Carretta et al. (2009) scale in the right panel. The figures illustrate the well-known dichotomy presented by the MW GCs: moderately metal-poor GCs tend to group around $\langle P_{ab} \rangle \sim 0.55$ days, while very metal-poor GCs preferentially have $\langle P_{ab} \rangle \sim 0.65$ days. Clearly visible is the region avoided by the GGCs, which spans the period range 0.58 days $\lesssim \langle P_{ab} \rangle \lesssim$ 0.62 days and is usually referred to as the "Oosterhoff gap" (e.g., Catelan 2004, 2009). According to the metallicity adopted in the present study ([Fe/H] = −1.59 or −1.60 dex in the Zinn & West 1984 and the Carretta et al. 2009 metallicity scale, respectively), G11 (asterisk in Figure 10) locates in the "transition" region where, in the MW, one finds GCs on both sides of the Oosterhoff-gap, i.e., GCs that have almost the same metal abundance, yet very different $\langle P_{ab} \rangle$ values. The rather long mean period of its RRab stars clearly places G11 in the Oo II region of the plot, in perfect agreement with its blue HB.

The Bailey (period–amplitude) diagram has also been proposed as an indicator of the Oosterhoff typology (Clement & Shelton 1999). In this diagram, RRL stars belonging to the two different Oosterhoff groups appear well separated: For a given amplitude (which corresponds to a given temperature), Oo II RRL stars show longer periods than Oo I variables. The usually adopted Oo I locus has been derived using RRL stars belonging to the GC M3 and both the linear (Clement & Rowe 2000) and the nonlinear (Cacciari et al. 2005) relations well represent most of the Oo I GGCs. The Oo II relation is less well defined. Clement & Rowe (2000) derived an Oo II locus using the metal-poor RRL stars in the GC ω Centauri. However, this cluster is well known to be a peculiar object (see, e.g., Sollima et al. 2005), which might be the core of a stripped dwarf spheroidal galaxy (e.g., Dinescu 2002; Lee et al. 2002; Altmann et al. 2005; Meza et al. 2005; Bekki & Norris 2006; Villanova et al. 2007; Wylie-de Boer et al. 2010; Majewski et al. 2012). On the other hand, Cacciari et al. (2005) found that their Oo I quadratic relation, shifted by $\Delta \log P \sim 0.06$ days (at fixed amplitude) to match the evolved stars in M3, also corresponds approximately to the mean locus traditionally assigned to the Oo II variables (Sandage et al. 1981). However, we suspect that none of these relations are fully representative of the Oo II GGCs. In order to compare the M31 GCs with a relation that better represents the Oo II GGCs, R. Contreras Ramos (2013, in preparation) obtained a new Oo II locus by fitting the periods and amplitudes of more than 190 fundamental-mode RRL stars belonging to the 19 Oo II clusters shown in Figure 10 (right panel), excluding known Blazhko (Blazhko 1907) and
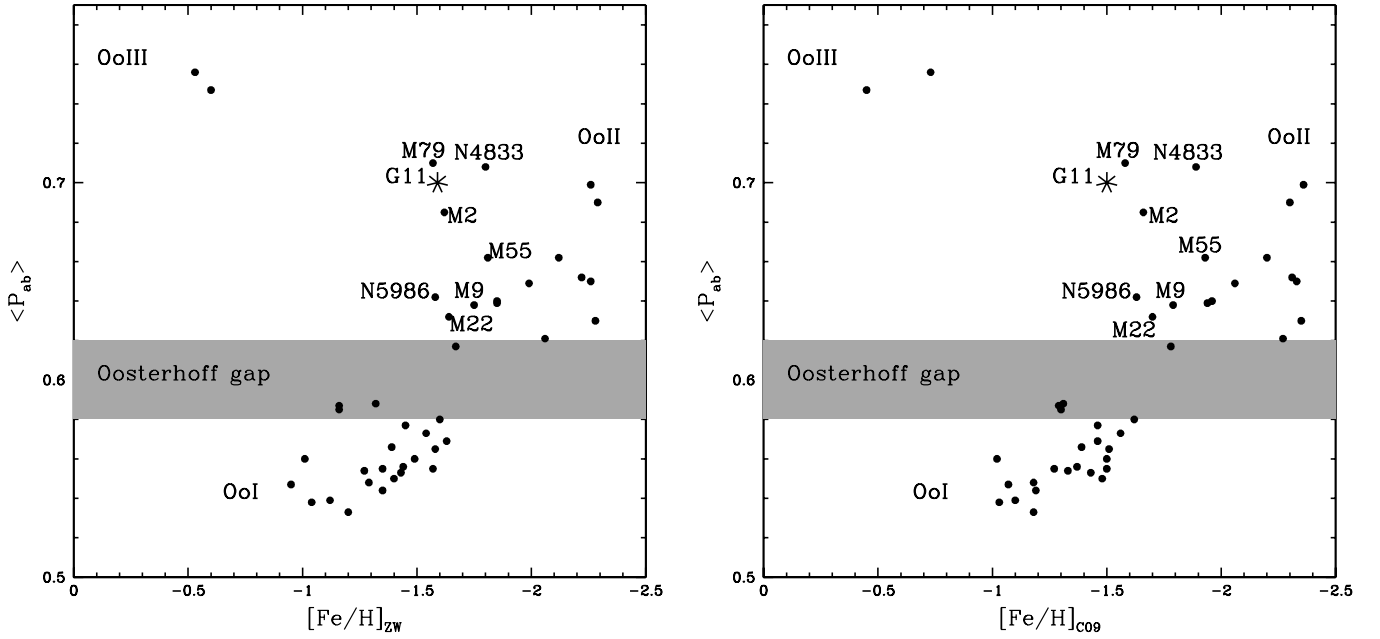
Figure 10. Mean period of the RRab stars against metallicity for the MW GCs (dots) containing RRL stars, showing the well known Oosterhoff dichotomy. G11 (asterisk) is located in the Oo II region. Metallicities in the left and right panels are in the Zinn & West (1984) and in the Carretta et al. (2009) scales, respectively. All the GCs shown in the figure contain five or more RRab stars, except M55 which has only four. The two Oo III clusters are NGC 6388 and NGC 6441.
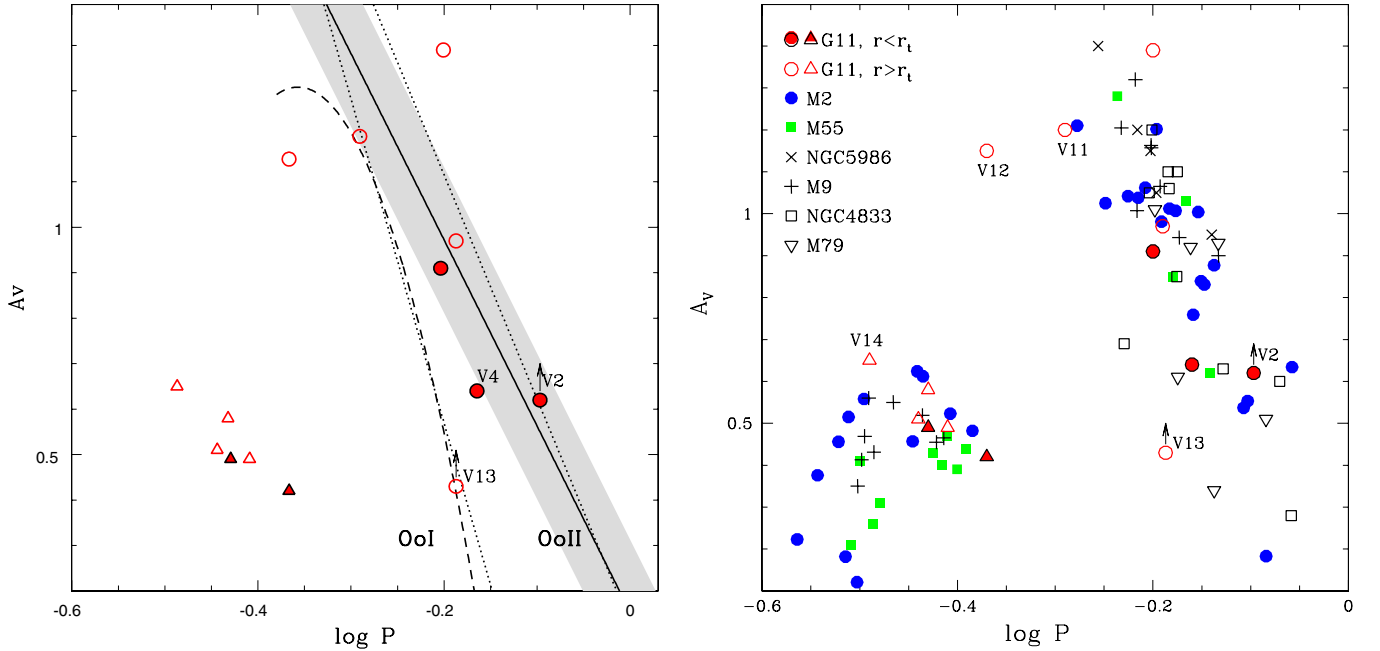

Figure 11. Left panel: V-band period–amplitude (Bailey) diagram for the RRL stars identified in this study. Symbols and color-coding are the same as in Figures 3 and 5. The dotted lines show the loci of the Oo I and Oo II GGCs according to Clement & Rowe (2000). The dashed curve represents the locus of the Oo I GGCs derived by Cacciari et al. (2005) based on the RRL stars in M3. The solid line shows a new locus for Oo II GCs derived using more than 190 RRab stars in 19 Oo II GGCs (R. Contreras Ramos 2013, in preparation). The gray region represents the 1σ confidence levels of the new relation. Right panel: comparison of G11 RRL stars with variables in the Oo II GGCs M2 (Clement et al. 2001), M55 (Clement et al. 2001), NGC 5986 (Alves & Onken 2001), M9 (Clement & Shelton 1999), NGC 4833 (Darragh & Murphy 2012), and M79 (Kains et al. 2012).

(A color version of this figure is available in the online journal.)

blended stars. The new Oo II locus is represented by the linear relation: $A_V(\mathrm{RRab}) = 0.15(\pm 0.05) - 4.10(\pm 0.25)\log P_{ab}$ (with $\sigma = 0.16$ mag and a correlation coefficient of 0.76) and is plotted as a solid line in the left panel of Figure 11 along with the RRL stars detected in the present paper. The position of the G11 RRab stars is very consistent with the new Oo II line. In the right panel of Figure 11 we compare the G11 RRL stars with the individual variables belonging to the Oo II GGCs with

most similar metallicity, as shown in Figure 10. Fundamental-mode and first overtone RRLs in all these clusters occupy the same regions of the Bailey diagram with only very few exceptions. In conclusion, according to all the pulsation indicators ($\langle P_{ab} \rangle$, $\langle P_c \rangle$, N_c/N_{ab}, and the location in the $\langle P_{ab} \rangle - $ [Fe/H] and period–amplitude planes) G11 appears to be a pure Oosterhoff type II GC, comparable to the GCs to similar properties (HB morphology and [Fe/H]) observed in the MW.
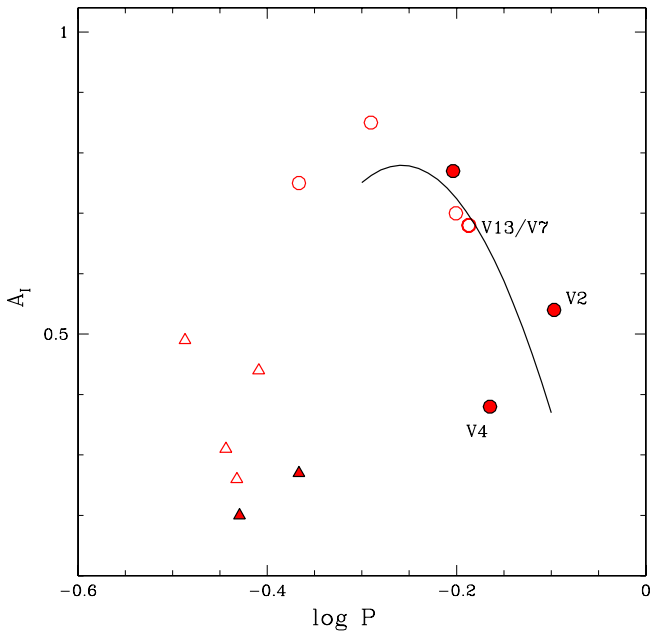
Figure 12. *I*-band period–amplitude diagram of the G11 RRL stars. Symbols and color-coding are the same as in Figures 3, 5, and 11. The solid curve represents the locus of the RRLs in the Oo II GC M53 derived by Arellano Ferro et al. (2011).

(A color version of this figure is available in the online journal.)

Three of the variable stars outside the tidal radius of G11 fall close to the Oo I locus (see left panel of Figure 11). They are V11, V12, and V13. V11 and V12 have short periods of 0.51 and 0.43 days, respectively, which are consistent with an Oo I classification. They are among the most external RRLs we have identified in our FOV and likely belong to the field of M31, which is know to have Oo I properties (see, e.g., Brown et al. 2004; Sarajedini et al. 2009; Jeffery et al. 2011). The period of V13, $P = 0.65$ days, suggests an Oo II classification, but the rather small visual amplitude places this star closer to the Oo I line. However, the visual amplitude of V13 appears to be smaller than its red *I*-band amplitude. In Figure 12 we show the *I*-band period–amplitude diagram of all the G11 RRL stars and compare it with the Oo II locus by Arellano Ferro et al. (2011). The position of V13 appears to be fully consistent with the *I*-band Oo II locus, thus suggesting that the star may be contaminated by a companion and its *V*-band amplitude reduced by blending. The same conclusion can be applied to V4, which was noted in Section 5.2 to be too blue for its period and brighter than the other G11 RRL stars.

5.4. Distance to G11

The distance to G11 was derived, along with the cluster metallicity and reddening, by fitting the cluster red giant and horizontal branches to the ridgelines of well-studied GGCs. Figure 13 shows the results obtained by fitting the CMD of G11, from the sources imaged on the PC, to the ridgelines of the GGCs 47 Tuc ([Fe/H] $= -0.71/-0.76$ dex, where the first metallicity value is on the Zinn & West 1984 scale and the second value is on the Carretta et al. 2009 scale); M5 ([Fe/H] $= -1.4/-1.33$ dex); M3 ([Fe/H] $= -1.66/-1.50$ dex); M15 ([Fe/H] $= -2.15/-2.33$ dex); and M92 ([Fe/H] $= -2.24/-2.35$ dex). References for the GGC CMDs can be found in Federici et al. (2012), who also provide an exhaustive description of the fitting procedure. The CMD of G11 is best fitted by the ridgeline of the GGC M3 for $E(B - V) = 0.12$ mag, and
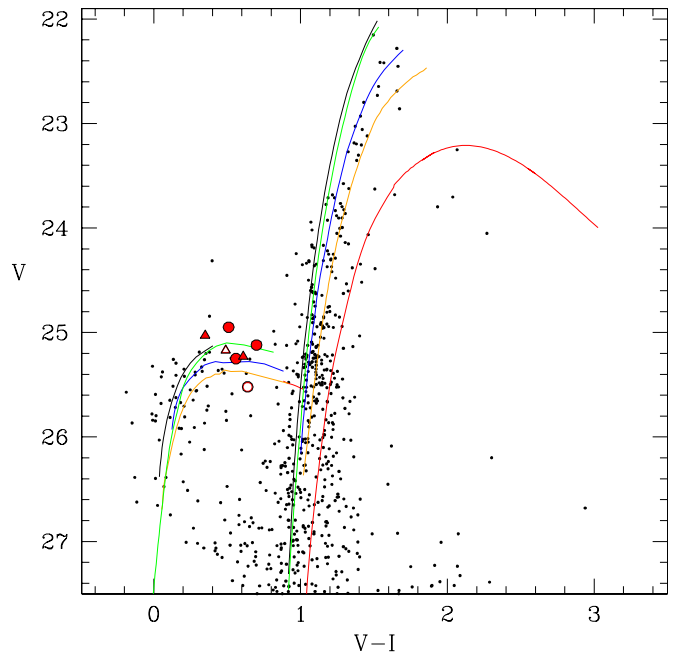

Figure 13. Fit of the CMD, from sources within the cluster tidal radius, to the ridgelines of the GGCs (from red to black): 47 Tuc ([Fe/H] $= -0.71$ dex); M5 ([Fe/H] $= -1.4$ dex); M3 ([Fe/H] $= -1.66$ dex); M15 ([Fe/H] $= -2.15$ dex); and M92 ([Fe/H] $= -2.24$ dex). All metallicities are on the Zinn & West (1984) metallicity scale.

(A color version of this figure is available in the online journal.)

a distance modulus of $(m - M)_0 = 24.46 \pm 0.10$ mag (corresponding to $D = 780 \pm 72$ kpc), in good agreement, within the errors, with the M31 modulus derived by Riess et al. (2012) and the distance to G11 derived by Federici et al. (2012). Figure 13 shows that the average luminosity of the G11 RR Lyrae stars on the PC is reasonably well fitted by the M3 HB, however, as pointed out at the end of Section 5.2, two of the cluster RR Lyrae stars (namely, V1 and V4) are rather overluminous, and the remaining three variables within the cluster tidal radius (V2, V3, and V5) also lead to an average luminosity of $\langle V(RR) \rangle = 25.20$ mag ($\sigma = 0.07$ mag, average on three stars) that is about 0.17 mag brighter than the mean HB magnitude obtained by fitting the cluster CMD with the ridgeline of M3. Blending and contamination by companions in the crowded central regions of G11 may be responsible for the high luminosities of the RR Lyrae stars within the cluster tidal radius, particularly in the case of V1 and V4. In this respect it is worth noting that $\langle V(RR) \rangle$ becomes fainter with increasing distance from the cluster center (see Figure 14), and in fact the average magnitude of the four most external variables (namely, V11, V12, V13, and V14) is 25.38 mag ($\sigma = 0.05$ mag, average on four stars), in good agreement with the value of $\langle V(HB) \rangle = 25.37$ mag obtained by the fit with M3. Furthermore, the rather blue HB morphology of G11 also suggests that the cluster RR Lyrae stars might be overluminous because they are evolved off the zero-age horizontal branch (ZAHB). Both the aforementioned effects may conspire to produce the enhanced luminosities observed for the G11 RR Lyrae stars and caution against using these variables to estimate the cluster distance.

6. SUMMARY AND CONCLUSIONS

We have performed a study of the variable star population of the globular cluster G11 based on WFPC2/*HST* time-series data
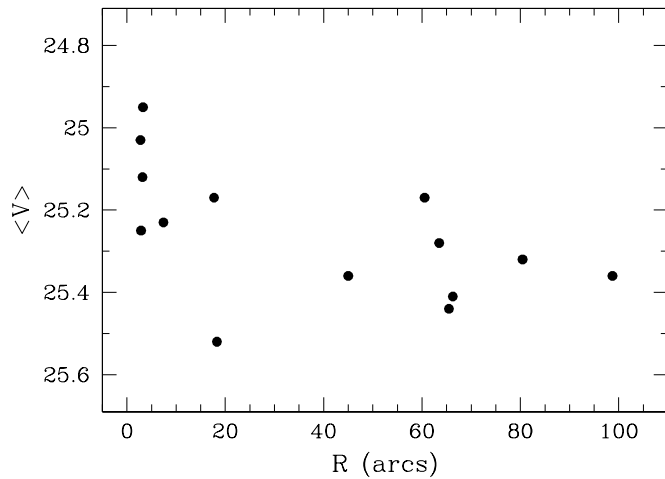
Figure 14. Run of the mean luminosity of the individual RR Lyrae stars, $\langle V(RR) \rangle$, with increasing the distance from the cluster center.

properly scheduled in order to detect and characterize the RRL variable star population of this M31 cluster. A main purpose of this study was to verify whether the Oosterhoff dichotomy exists in the Andromeda galaxy. We summarize our results in the following.

1. We have identified 14 variable stars, all belonging to the RRL class, in the $150'' \times 150''$ total FOV covered by our WFPC2 observations. Five of them (three RRab's and two RRc's) are placed within the tidal radius of G11 (e.g., $r < 16''$), thus making them very likely cluster members. The remaining RRL stars are located at distances in the range of $17''.7$–$98''.7$ from the cluster center, and may in part represent the M31 field variable star population.

2. The G11 CMD shows that the cluster HB is quite extended in color, stretching across the IS, and extending significantly to the blue through a tail that reaches $V \sim 26$ mag at $V - I \sim 0.2$ mag, shows a gap, and then an extremely blue tail formed by stars with $V \geqslant 26.3$ mag and $V - I \lesssim 0.2$ mag, likely belonging to the G11's HB, since this same feature is lacking in the control fields.

3. The distance to G11 was derived by fitting the cluster red giant and horizontal branches, from the sources imaged on the PC, to the ridgelines of well-studied GGCs. The CMD of G11 is best fitted by the ridgeline of the GGC M3 for $E(B - V) = 0.12$ mag, and a distance modulus of $(m - M)_0 = 24.46 \pm 0.10$ mag.

4. The average luminosity of the G11 RRL stars on the PC is reasonably well fitted by the M3 HB; however, two of the cluster RRL stars (namely, V1 and V4) are rather overluminous, and the remaining three variables within the cluster tidal radius also lead to an average luminosity that is about 0.17 mag brighter that the mean HB magnitude obtained by fitting the cluster CMD with the ridgeline of M3. Blending and contamination by companions in the crowded central regions of G11, along with evolution off a position on the blue ZAHB, given the rather blue HB morphology of G11, likely conspire to produce the enhanced luminosities observed for the G11 RR Lyrae stars and caution against using these variables to estimate the cluster distance.

5. Using the three RRab cluster members, we find $\langle P_{ab} \rangle = 0.70$ days and $P_{ab,\text{min}} = 0.626$ days. Both quantities qualify G11 as an Oo II GC. The position of G11 in the period–

[Fe/H] and period–amplitude diagrams further supports its Oo II nature and confirms the importance of the HB morphology in the Oosterhoff classification.

To conclude, we have found the first evidence that Oosterhoff type II GCs exist in the Andromeda galaxy and seem to follow the same rule of their MW counterparts, where moderately metal-poor ([Fe/H] ~ -1.6) GCs with a blue HB, and containing RRL stars show Oo II properties.

REFERENCES

Altmann, M., Catelan, M., & Zoccali, M. 2005, A&A, 439, L5
Alves, D. R., Bond, H. E., & Onken, C. 2001, AJ, 121, 318
Arellano Ferro, A., Figuera, J. R., Giridhar, S., et al. 2011, MNRAS, 416, 2265
Baldacci, L., Rizzi, L., Clementini, G., & Held, E. V. 2005, A&A, 431, 1189
Barning, F. J. M. 1963, BAN, 17, 22
Bekki, K., & Norris, J. E. 2006, ApJL, 637, L109
Bellazzini, M., Cacciari, C., Federici, L., Fusi Pecci, F., & Rich, M. 2003, A&A, 405, 867
Blazhko, S. 1907, AN, 175, 325
Bonoli, F., Delpino, F., Federici, L., & Fusi Pecci, F. 1987, A&A, 185, 25
Brown, T. M., Ferguson, H. C., Smith, E., et al. 2004, AJ, 127, 2738
Cacciari, C., Corwin, T. M., & Carney, B. W. 2005, AJ, 129, 267
Caputo, F., Castellani, V., Marconi, M., & Ripepi, V. 2000, MNRAS, 316, 819
Carretta, E., Bragaglia, A., Gratton, R., & Lucatello, S. 2009, A&A, 505, 139
Catelan, M. 2004, in ASP Conf. Ser. 310, IAU Colloquium 193: Variable Stars in the Local Group, ed. D. W. Kurtz & K. R. Pollard (San Francisco, CA: ASP), 113
Catelan, M. 2009, Ap&SS, 320, 261
Catelan, M., Greco, C., Amigo, P., et al. 2012, AJ, submitted
Clement, C. M., Muzzin, A., Dufton, Q., et al. 2001, AJ, 122, 2587
Clement, C. M., & Rowe, J. 2000, AJ, 120, 2579
Clement, C. M., & Shelton, I. 1999, ApJL, 515, L85
Clementini, G. 2010, in Variable Stars, the Galactic Halo and Galaxy Formation, ed. C. Sterken, N. Samus, & L. Szabados (Moscow: Sternberg Astronomical Inst.), 107
Clementini, G., Contreras, R., Federici, L., et al. 2009, ApJL, 704, L103
Clementini, G., Di Tomaso, S., Di Fabrizio, L., et al. 2000, AJ, 120, 2054
Clementini, G., Federici, L., Corsi, C., et al. 2001, ApJL, 559, L109
Contreras Ramos, R. 2010, PhD thesis, Univ. Bologna, Dep. Astronomy
Cseresnjes, P. 2001, A&A, 375, 909
Darragh, A. N., & Murphy, B. W. 2012, JSARA, 6, 72
Dinescu, D. I. 2002, in ASP Conf. Ser. 265, Omega Centauri, A Unique Window into Astrophysics, ed. F. van Leeuwen, J. D. Hughes, & G. Piotto (San Francisco, CA: ASP), 365

Dolphin, A. E. 2000, PASP, 112, 1383
Fan, Z., de Grijs, R., & Zhou, X. 2010, ApJ, 725, 200
Federici, L., Cacciari, C., Bellazzini, M., et al. 2012, A&A, 544, 155
Fiorentino, G., Contreras Ramos, R., Clementini, G., et al. 2010a, ApJ, 711, 808
Fiorentino, G., Contreras Ramos, R., Tolstoy, E., Clementini, G., & Saha, A. 2012, A&A, 539, 138
Fiorentino, G., Monachesi, A., Trager, S. C., et al. 2010b, ApJ, 708, 817
Galleti, S., Bellazzini, M., Buzzoni, A., Federici, L., & Fusi Pecci, F. 2009, A&A, 508, 1285
Galleti, S., Federici, L., Bellazzini, M., Fusi Pecci, F., & Macrina, S. 2004, A&A, 416, 917
Helmi, A., Irwin, M. J., Tolstoy, E., et al. 2006, ApJL, 651, L121
Holtzman, J. A., Burrows, C. J., Casertano, S., et al. 1995, PASP, 107, 1065
Huchra, J. P., Brodie, J. P., & Kent, S. M. 1991, ApJ, 370, 495
Jeffery, E. J., Smith, E., Brown, T. M., et al. 2011, AJ, 141, 171
Kains, N., Bramich, D. M., Figuera Jaimes, R., et al. 2012, A&A, 548, A92
Lafler, J., & Kinman, T. D. 1965, ApJS, 11, 216
Lee, Y.-W., Rey, S.-C., Ree, C. H., et al. 2002, in ASP Conf. Ser. 265, Omega Centauri, A Unique Window into Astrophysics, ed. F. van Leeuwen, J. D. Hughes, & G. Piotto (San Francisco, CA: ASP), 305
Lomb, N. R. 1976, Ap&SS, 39, 447
Majewski, S. R., Nidever, D. L., Smith, V. V., et al. 2012, ApJL, 747, L37
Mancone, C., & Sarajedini, A. 2008, AJ, 136, 1913
Meza, A., Navarro, J. F., Abadi, M. G., & Steinmetz, M. 2005, MNRAS, 359, 93
Miceli, A., Rest, A., Stubbs, C. W., et al. 2008, ApJ, 678, 865

Oosterhoff, P. T. 1939, Obs, 62, 104
Oosterhoff, P. T. 1944, BAN, 10, 55
Preston, G. W. 1959, ApJ, 130, 507
Pritchet, C. J., & van den Bergh, S. 1987, ApJ, 316, 517
Pritzl, B. J., Armandroff, T. E., Jacoby, G. H., & Da Costa, G. S. 2002, AJ, 124, 1464
Pritzl, B. J., Armandroff, T. E., Jacoby, G. H., & Da Costa, G. S. 2004, AJ, 127, 318
Pritzl, B. J., Armandroff, T. E., Jacoby, G. H., & Da Costa, G. S. 2005, AJ, 129, 2232
Rich, R. M., Corsi, C. E., Cacciari, C., et al. 2005, AJ, 129, 2670
Riess, A. G., Fliri, J., & Valls-Gabaud, D. 2012, AJ, 745, 156
Sandage, A., Katem, B., & Sandage, M. 1981, ApJS, 46, 41
Sarajedini, A., Mancone, C. L., Lauer, T. R., et al. 2009, AJ, 138, 184
Sarajedini, A., Yang, S.-C., Monachesi, A., Lauer, T. R., & Trager, S. C. 2012, MNRAS, 425, 1459
Sawyer, H. B. 1944, PDDO, 1, 294
Shetrone, M. D., Coté, P., & Sargent, W. L. W. 2001, ApJ, 548, 592
Smith, H. A. 1995, RR Lyrae Stars (Cambridge Astrophysics Series; Cambridge: Cambridge Univ. Press)
Sollima, A., Pancino, E., Ferraro, F. R., et al. 2005, ApJ, 634, 332
Stellingwerf, R. F. 1978, ApJ, 224, 953
Stetson, P. B. 1996, PASP, 108, 851
Villanova, S., Piotto, G., King, I. R., et al. 2007, ApJ, 663, 296
Welch, D. L., & Stetson, P. B. 1993, AJ, 105, 1813
Wylie-de Boer, E., Freeman, K., & Williams, M. 2010, AJ, 139, 636
Zinn, R., & West, M. J. 1984, ApJS, 55, 45